ACS APPLIED OPTICAL MATERIALS

Open Access

This article is licensed under CC-BY 4.0

pubs.acs.org/acsaom

Article

Quantifying the Open Time and Film Formation of Waterborne Coatings with Laser Speckle Imaging

Slav A. Semerdzhiev, Hanne M. van der Kooij, Remco Fokkink, Jasper van der Gucht, and Joris Sprakel*

Cite This: ACS Appl. Opt. Mater. 2024, 2, 750−760

Read Online

ACCESS | Metrics & More | Article Recommendations | Supporting Information

ABSTRACT: In drying waterborne paints, the time span between the deposition of the liquid dispersion and the formation of a uniform solid film harbors a procession of complex phenomena each of which determines the final properties of the dry paint film. One of the major challenges in the design of sustainable, water-based paints is to match or surpass the drying performance of their solvent-based counterparts. In particular, the so-called "open time"—the time during which the paint remains wet and susceptible to alterations without affecting the aesthetics of the final film—is often much shorter in waterborne systems than in solvent-borne equivalents. This short time window hastens the painter, limits remodeling of defects, and makes it difficult to smoothly blend the edges of a previously and freshly deposited paint without introducing permanent brush marks. Optimizing and tailoring the open time is thus desired. This endeavor would greatly benefit from methods capable of determining this critical parameter in a fast and objective way. Yet, experimental access to the internal dynamics accompanying the drying process is challenging. Paints are often opaque, which precludes the use of traditional optical methods. Additionally, the drying phenomena usually populate a multitude of time and length scales. To address these obstacles, we deploy the optical technique laser speckle imaging (LSI), which allows probing nanoscale motions deep inside turbid paints. We apply this method to quantitatively and objectively determine the open time. We develop a set of scaling relations that accurately predict the experimentally measured open time as a function of key parameters governing the drying process. Additionally, we harness the wide temporal dynamic range of LSI to capture phenomena that occur during the later drying stages, including deformation and coalescence of the polymer particles.

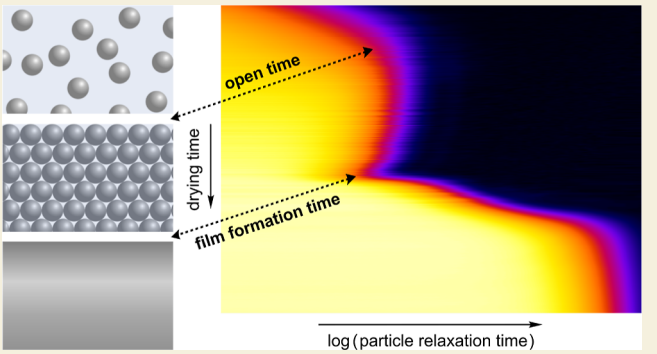

KEYWORDS: *open time, water-based paints, laser speckle imaging, dispersion drying, film formation*

1. INTRODUCTION

The drying of aqueous colloidal coatings has been subject to scientific scrutiny for many decades. The entanglement of numerous accompanying phenomena such as hydrodynamics, colloidal interactions, and mechanics renders the drying process highly complex and has prompted significant research efforts in pursuit of a better understanding. The need of such also has a practical genesis: drying composite colloidal coatings are of great importance for a variety of industrial fields such as food technology, inkjet printing, and particularly coatings technology.[1−3] Solvent-based coatings emit volatile organic compounds (VOCs), which are very potent in amplifying the greenhouse effect and additionally are hazardous to the health of the consumer and the professional applying the coating.[4−7] These issues have prompted a transition from solvent-borne coatings to solvent-free or water-based (latex) systems. However, such a transition is far from trivial and offers many challenges. Water-based paints often dry much faster than their solvent-borne equivalents. This significantly shortens the time window in which the deposited paint can be handled without leaving topological irregularities; a crucial parameter for paints, known as the open time. Moreover, in the drying stages of water-based paints that are successive to the open time period, the binder particles must coalesce to achieve phase inversion and film formation. The timing of this stage is also critical as it determines the properties of the final film.

The dynamics underlying the drying process determine the visual appearance, mechanical properties, and barrier properties of the dry paint. The first step toward solving the challenges listed above is establishing the right tool to study and interpret these drying dynamics. That is a challenge in itself. Studying the dynamics is notoriously difficult as they are often spatiotemporally heterogeneous and span a wide range of

Received: January 30, 2024
Revised: April 15, 2024
Accepted: April 23, 2024
Published: May 14, 2024

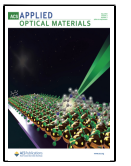

Downloaded via WAGENINGEN UNIV & RESEARCH on June 18, 2024 at 09:48:47 (UTC).
See https://pubs.acs.org/sharingguidelines for options on how to legitimately share published articles.

© 2024 The Authors. Published by American Chemical Society

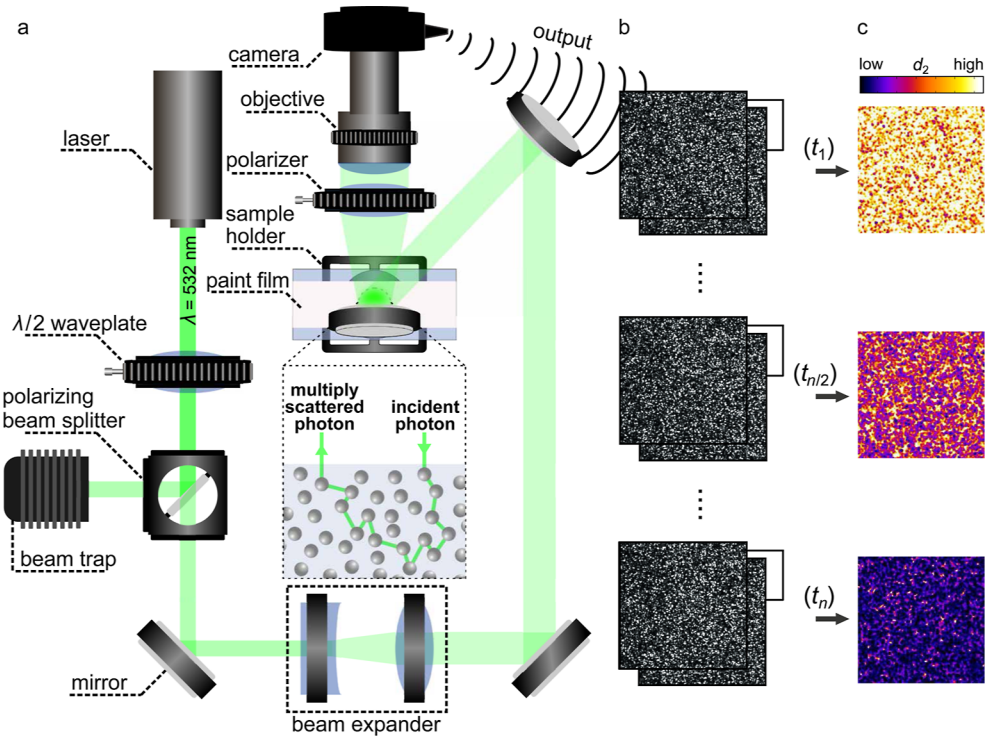

Figure 1. LSI setup and output. (a) Schematic of the LSI instrument. The light is guided to the drying aqueous coating and impinges on it. (Inset) After multiple scattering events (green broken line), the propagation direction of photons in the sample is completely randomized. The multiply scattered light emanating from the sample is subsequently collected and projected onto a CCD camera chip. This yields a sequence recording of speckle patterns (b). Correlating the raw speckle images using eq 1 at a fixed correlation time τ for different time points t_i (i = 1..n) during the drying process translates the raw data into dynamic d_2 maps (c). In the beginning of the drying process (t_1), the coating is populated with high dynamics, while at the mid-drying stage ($t_{n/2}$) the dynamics have significantly slowed down due to the ongoing evaporation. At the end (t_n), all dynamics on the time scale of τ have been brought to a halt. Each image in (b,c) is 2 × 2 mm^2.

time and length scales, which places a demand for methods that offer both high spatial and temporal resolution. Additionally, the high turbidity of paints precludes investigations relying on conventional techniques such as microscopy (bright-field or fluorescence-based) and dynamic light scattering that only work for sufficiently transparent samples, which coatings rarely are.

The limited availability of proper means to monitor and study paint drying obscures the progress in optimizing this process and makes it difficult to determine with high fidelity important quantities such as the open time and film formation time. Existing methods for drying time determination, such as the finger touch test and the mechanical straight-line drying-time recorder, are subjective and prone to human error due to variations in pressure applied or instrument design. While recorder methods offer a more standardized approach, variations in testing conditions across laboratories can significantly impact results. For instance, some standards, like ISO 9117-4, allow for user-defined coating thickness, while others, like ASTM D5895, recommend specific thicknesses based on paint type. Additionally, lighting conditions can play a crucial role in the deduced drying time. These inconsistencies lead to difficulties in comparing results obtained using different methods or by different operators. Furthermore, traditional methods for open time determination, such as brushing a fresh layer of coating onto a partially dried film and relying on visual assessment of merging, are also susceptible to operator bias.[8] Sophisticated MRI-based approaches, while more precise and quantitative, are very expensive and not readily accessible.[9,10] These limitations necessitate the development of a more objective, quantitative, and universally applicable method to study paint drying dynamics.

In this work, we use laser speckle imaging (LSI) as a relatively inexpensive and straightforward approach to elucidate with microscopic resolution the dynamics inside drying opaque latex coatings, spanning 7 orders of magnitude in time. Access to these internal dynamics allows us to measure the open time of realistic paint formulations in a quantitative and objective manner and for a wide range of conditions. We then use our LSI method to systematically investigate the dependence of the open time on different environmental parameters, such as humidity and temperature, and interpret these results using a model for diffusion-limited evaporation. Finally, we further expand the application scope of LSI by demonstrating its ability to follow in detail the film formation in later drying stages. Not only can we detect the likely onset of phase inversion, but we can also track the dependence of this phenomenon on an important parameter such as the hardness of the latex particles. This method makes it possible to time-stamp critical stages in the drying of a latex coating with a high degree of accuracy, offering new handles for the rational design of improved water-based paint formulations.

2. RESULTS AND DISCUSSION

2.1. Laser Speckle Imaging

LSI exploits multiple light scattering to evaluate, with both high temporal and spatial resolution, the dynamics inside opaque materials. This characteristic feature has encouraged the deployment of LSI in numerous fields such as biology, food

https://doi.org/10.1021/acsaom.4c00051
ACS Appl. Opt. Mater. 2024, 2, 750−760

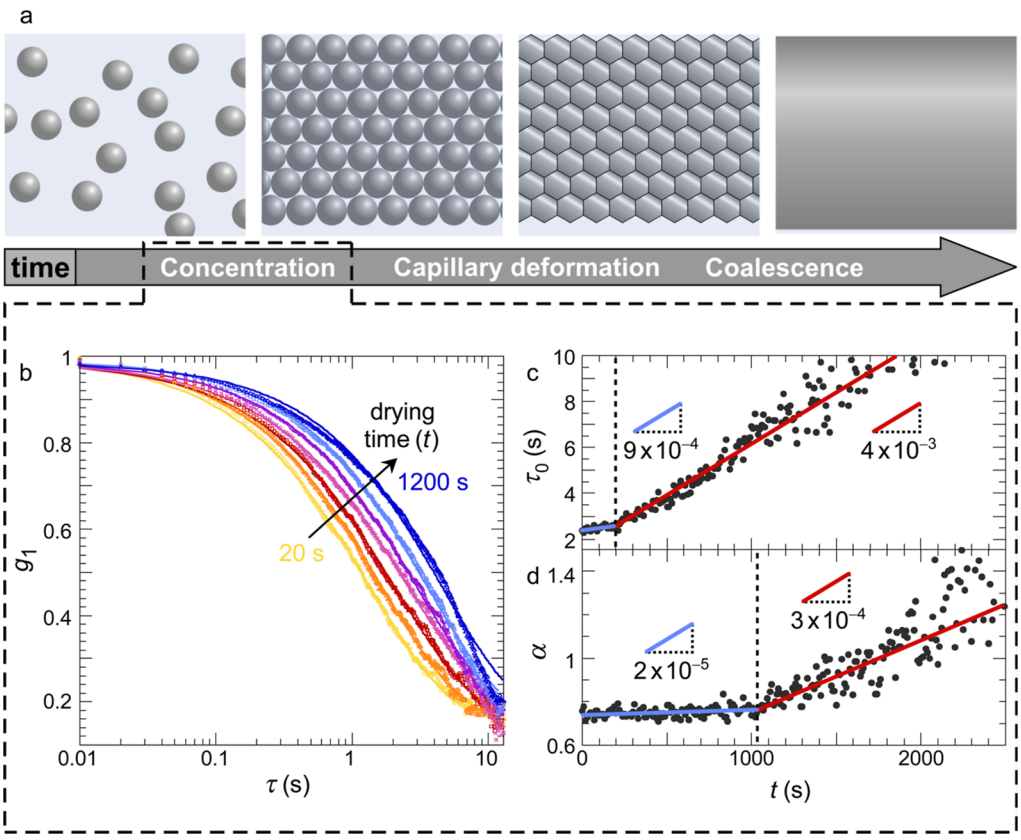

Figure 2. Open-time determination with LSI. (a) Simplified schematic of the main events taking place in a drying aqueous coating of soft colloidal particles. (b) Typical temporal evolution of the field correlation function g_1. The curves shift toward longer correlation times τ due to evaporation-induced particle concentration. The solid lines are fits to eq 4. (c) Changes in the relaxation time τ_0 and the (d) process identifier α with the progression of the drying process. The temporal evolution of both parameters can be divided into two distinct regimes demarcated by a dashed line and colored (solid lines) in blue or red. The slopes (⟋) $d\tau_0/dt$ and $d\alpha/dt$ are colored in accordance with the corresponding regime. For $\tau_0(t)$, the dashed line marks the start of a sudden and more steep increase of the effective viscosity and thus the onset of deterioration of the coating workability. In the case of $\alpha(t)$, the dashed line designates an abrupt change, signaling the formation of a semisolid film. We consider this time point as the upper bound of t_{OT}.

technology, materials science, and surface science.[11−24] In a turbid medium, light propagates via multiple scattering events. After a certain number of such events, the propagation direction of the photons is completely randomized (Figure 1a, inset). This allows us to treat photon propagation in an opaque medium as a diffusive transport.[25] At the detector, the scattered photons emanating from the sample superpose and generate a speckle pattern (Figure 1b) due to interference of the different paths that they have traversed. Since light diffuses orders of magnitude faster than any molecular or particle translational motion, the momentary realization of this interference pattern is directly related to the instantaneous arrangement of the scattering species within the sample. At longer time scales, the speckle pattern changes because of the displacement of the scattering particles. LSI uses the diffusive nature of light propagation in turbid systems to extract information from these temporal changes in the speckle patterns about the movement of scattering species, and thus about the ongoing internal dynamics.[26] To quantify the speckle intensity fluctuations, we use the intensity structure function d_2, defined as[27,28]

$$d_2(t, x, y, \tau) = \frac{\langle [I(t, x, y) - I(t + \tau, x, y)]^2 \rangle}{\langle I(t, x, y) \rangle \langle I(t + \tau, x, y) \rangle} \quad (1)$$

Here, t is the time passed since the moment of paint application, x and y are the spatial coordinates, and τ is the correlation time that sets the time lag between two speckle patterns that are compared. d_2 represents the decorrelation of speckle patterns and is thus a measure for the amount of change that has occurred in the scatterer arrangement due to motion after a time τ (Figure 1c). In samples with a high particle mobility, e.g., in the wet stages, d_2 values are high, while for samples in which scatterer motion is brought to a halt, as is the case in dried films, d_2 values are low. In this way, d_2 is a quantitative measure for the internal mobility inside the paint film and thus enables temporal and spatial mapping of the dynamics in it. Additionally, by choosing the appropriate τ, we can resolve processes that take place at different time scales. The ability to construct spatiotemporal d_2 maps allows us to monitor the evolution of the dynamics and easily detect any dynamic heterogeneity that may occur within the sample under investigation. Note that d_2 trumps the performance of the conventional intensity correlation function g_2 when statistics are limited,[28,29] which is inevitable for single-pixel intensity traces. In the absence of discernible inhomogeneities, however, we can average over all 640 × 480 pixels in the field of view to acquire abundant statistics and rely on g_2 instead. The intensity correlation function is defined as

https://doi.org/10.1021/acsaom.4c00051
ACS Appl. Opt. Mater. 2024, 2, 750−760

$$g_2(t, x, y, \tau) = \frac{\langle I(t, x, y)I(t + \tau, x, y)\rangle}{\langle I(t, x, y)\rangle\langle I(t + \tau, x, y)\rangle} \quad (2)$$

d_2 and g_2 are closely related through $d_2(t, x, y, \tau) = 2(g_2(t, x, y, 0) - g_2(t, x, y, \tau))$.[28] The spatially averaged $g_2(t, \tau) = \langle I(t)I(t + \tau)\rangle_{x,y}/(\langle I(t)\rangle_{x,y}\langle I(t + \tau)\rangle_{x,y})$ grants us more direct and intuitive access to the electric field correlation function g_1 via the Siegert relation

$$g_1(t, \tau) = \frac{1}{\sqrt{\beta}}\sqrt{g_2(t, \tau) - 1} \quad (3)$$

where β is a numerical prefactor dependent on the experimental setup (see the Experimental Section).[25] Finally, we fit $g_1(t, \tau)$ using a stretched exponential decay function

$$g_1(t, \tau) = \exp(-\gamma[\tau/\tau_0(t)]^{\alpha(t)}) \quad (4)$$

where $\tau_0(t)$ is the characteristic relaxation time, $\alpha(t)$ is a stretching (or compressing) exponent, and γ is an experimental numerical constant that has been determined elsewhere (see the Experimental Section). Both the relaxation time and stretching exponent are means to extract more quantitative information about the ongoing dynamics. For example, in the case of pure diffusion, the relaxation time is related to the diffusion coefficient D of the scatterers via $\tau_0 = 1/[6k_0^2D]$, where $k_0 = 2\pi n/\lambda_0$ is the wave vector with n the refractive index of the medium and λ_0 the laser wavelength in vacuum. In a nondilute solution with a complex composition, τ_0 provides information about the resistance, or what we will call effective viscosity throughout this work, that the scatterers experience while moving in such a complex environment. By contrast, the stretching exponent α reflects the type of motion that the scattering particles undergo and as such serves as "process identifier". Since $g_1(\tau) = \exp(-\gamma k_0\sqrt{\langle\Delta x^2(\tau)\rangle})$ with $\langle\Delta x^2(\tau)\rangle$ the mean-square displacement, it follows that $\langle\Delta x^2(\tau)\rangle \propto \tau^{2\alpha}$. Values of $\alpha < 0.5$ thus imply subdiffusive dynamics, $\alpha = 0.5$ signals Brownian dynamics, and $\alpha = 1$ indicates ballistic motion of the particles.[30,31] The complementary sensitivity of τ_0 and α to changes in the motion of the scattering particles makes these two quantities appropriate tools for monitoring the dynamics in evolving systems such as drying waterborne coatings. We note that the basis of our method forms the well-established diffusing wave spectroscopy,[25] which has been successfully applied to study drying stages in coatings using a commercial apparatus.[32−34] Our approach offers three key advancements: (i) we fit the entire correlation curves to extract both τ_0 and α, (ii) we perform spatially resolved analysis to account for possible heterogeneities, and (iii) we link our quantitative metrics to a model that validates our data under varying conditions.

2.2. Open Time of Waterborne Coatings

The drying of colloidal coatings is a complex phenomenon accompanied by a constellation of processes each of which is marked by its own characteristic dynamics, time scales, and length scales.[26,35,36] For soft colloids, the drying process can be divided into four main stages (Figure 2a). In the first stage, we have a liquid-like dispersion of freely diffusing particles. After some time, due to solvent evaporation, we enter the second stage in which the particles get concentrated and more densely packed. Upon close packing, capillary forces cause the particles to deform, which is marked as the third stage. Provided the glass transition temperature of the particle is sufficiently low, they coalesce to give a uniform film, which is the last (fourth) stage. The big temporal dynamic range of LSI allows us to capture different processes spanning multiple decades of time and thus many of the events that take place during the drying of such dispersions.[26] We first focus on the early drying stages of waterborne paint systems. The dynamics in these early stages govern the open time (t_{OT}) of the drying paint, which is a crucial handling parameter not only for paints but for any type of system containing an evaporating solvent. By definition, open time is the period after applying the paint in which the wet paint film can still be reworked without leaving any visible and permanent topographical irregularities. In other words, the open time marks the point in time where the initially liquid-like coating begins to display solid-like behavior.

To demonstrate that we can determine the open time in a quantitative and objective manner, we start by depositing a 200 μm thick coat of an acrylic−styrene emulsion paint on a glass substrate and record a sequence of raw speckle images of the central section of the drying paint. The formulation contains TiO_2 nanoparticles of relatively low concentration, yet sufficient to render the paint highly turbid and thus ensure optimal conditions for the deployment of LSI, i.e., multiple-scattering events. Since in such a setting, the TiO_2 nanoparticles are the dominant scattering species, they can be considered as reporters of the ongoing dynamics in the paint film, similarly to what is done in well-established microrheology approaches.[37] The resulting d_2 maps reveal spatially uniform evolution of the dynamics in time (Figure 1c), which justifies averaging the field correlation curves $g_1(\tau)$ over the entire field of view using eq 2 and (3). During water evaporation, the $g_1(\tau)$ curves shift toward longer correlation times τ (Figure 2b), which indicates retardation of the particle motion as a consequence of the increasing concentration. By examining the time evolution of the relaxation time τ_0 and the process identifier α, we can clearly discern different regimes in the dynamics. First, we focus on the concentration stage, in which the $\tau_0(t)$ curve exhibits a clearly visible change in the slope $d\tau_0/dt$ (Figure 2c). This characteristic kink signals a transition from a slow to a faster increase in the effective viscosity of the coating due to an increase in the particle packing fraction resulting from the water loss. We interpret this time point as the onset of deterioration in the workability of the coating. Interestingly, the $\alpha(\tau)$ curve shows a similar sudden increase in the slope $d\alpha/dt$ (Figure 2d). This kink, however, is shifted to a later time point and has a different origin. Even though not purely diffusive, the dynamics in the period preceding this time point $t < 1100$ s are more Brownian than advective ($\alpha \sim 0.7$) and barely change, whereas the subsequent period ($t > 1100$ s) gradually gets dominated by advective processes ($\alpha \to 1$). The transition between these distinct regimes marks the transformation of the liquid dispersion into a quasi-solid. Such a film with semisolid properties cannot be further reworked without leaving permanent defects. Bearing that in mind, we interpret this characteristic time point as our measure for the open time t_{OT} in the remainder of this paper.

2.3. Open Time versus Coating Thickness

Having established a quantitative determination of the open time of waterborne paints, we will couple this quantity to the evaporation rate of the film. Being successful in such an endeavor will not only validate our LSI findings but will also provide predictive power for the open time as a function of key

https://doi.org/10.1021/acsaom.4c00051
ACS Appl. Opt. Mater. 2024, 2, 750−760

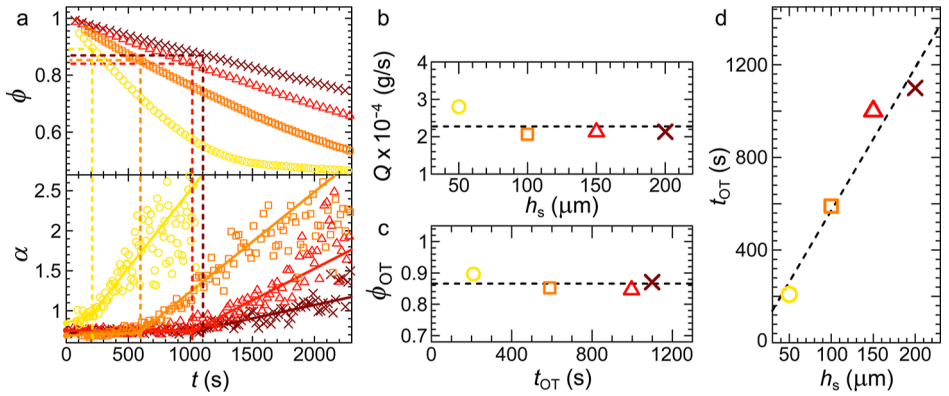

Figure 3. Open time as a function of coating thickness. (a) Normalized wet paint film mass (top) and process identifier (bottom) versus drying time for paint films with starting thickness h_S of 50 μm (yellow ○), 100 μm (orange □), 150 μm (red △), and 200 μm (brown ×). The dashed lines indicate the mass fractions at the end of the open time period ϕ_{OT}. The solid lines guide the eye through the different regimes in the $\alpha(t)$ curves and designate the open time t_{OT}. (b) Evaporation rate Q and (c) mass fraction ϕ_{OT} remain approximately constant for all coating thicknesses. Symbols represent the experimental data while the dashed lines are guides to the eye. (c) Open time versus coating thickness. The dashed line is a linear fit.

parameters influencing the drying process. The concentration and packing of particles are driven by the evaporation of water. Predicting the rate of evaporation is challenging, as different limiting factors may occur, such as diffusion in the liquid phase, thermal transfer at the interface, and diffusion and convection in the gas phase. In our experiments, a slow but steady air flow is applied over the sample to control the relative humidity, which leads to the formation of a boundary layer above the film−vapor interface.[38] In the case where the transfer of water molecules across the interface is fast, the air immediately above the interface is in equilibrium with the liquid film, and the evaporation rate is limited by diffusion of water molecules across the boundary layer. The diffusive flux is given by Fick's law, $J = D\Delta c/\delta$, with D the diffusivity of water in the boundary layer and $\Delta c/\delta$ the water concentration gradient across the boundary layer, where the thickness of the boundary layer δ is determined by the air flow in the chamber. This leads to an evaporative mass loss $Q = dM/dt$ given by

$$Q = A\frac{Dm}{kT}\frac{(p_{eq} - p_v)}{\delta} \tag{5}$$

where A is the total area of the applied paint film (which is kept constant in our experiments), p_{eq} and p_v denote the equilibrium vapor pressure immediately above the film and the vapor pressure in the chamber (outside the boundary layer), respectively, m is the mass of a water molecule, k is the Boltzmann's constant, and T is the temperature. In the other limit, where diffusion in the vapor phase is fast, the evaporation rate is limited by the transfer rate of molecules across the interface, which can be estimated using classical kinetic theory, leading to the Langmuir−Hertz−Knudsen equation[39−41]

$$Q = A\alpha_v(p_{eq} - p_v)\sqrt{\frac{m}{2\pi kT}} \tag{6}$$

where α_v is a sticking or evaporation coefficient ($0 \le \alpha_v \le 1$). While it is difficult to obtain values for δ and α_v and to assess which of the two scenarios applies in our experiments, eqs 5 and 6 show that in both limits, the evaporation rate is expected to be independent of the film thickness and proportional to the difference between the equilibrium vapor pressure and the actual vapor pressure, $p_{eq} - p_v$.

Experimentally, we can obtain the evaporation rate by monitoring the mass of the film in parallel with LSI. Figure 3a (top) shows the normalized mass, $\phi(t) = M(t)/M(0)$, as a function of time for different initial film thicknesses. The mass decreases linearly with time in the early stages, indicating a constant evaporation rate. Toward the end of the drying process, the water activity in the film decreases significantly, which leads to a decrease of p_{eq} and thereby a decrease in the evaporation rate. When $p_{eq} = p_v$, the drying stops. The initial evaporation rate Q is independent of the initial film thickness (Figure 3b), as expected from eqs 5 and 6. We also expect that the end of the open-time period occurs always at the same effective particle concentration, regardless of the initial thickness of the wet paint film. To test the validity of this conjecture, we evaluate the mass loss (Figure 3a, top) at the open time t_{OT}, as derived from the kink in the corresponding $\alpha(t)$ curves (Figure 3a, bottom). We indeed find that the mass fraction at the end of the open time period, ϕ_{OT}, does not depend on the initial film thickness (Figure 3c). From Figure 3a, we see, moreover, that the drying rate is constant during the open-time period, which means that we can estimate the open time as

$$t_{OT} = \frac{M(0) - M(t_{OT})}{Q} = \frac{M(0)(1 - \phi_{OT})}{Q} \tag{7}$$

Since Q and ϕ_{OT} are independent of the initial thickness h_s, and the initial mass is proportional to h_s, we expect that t_{OT} increases linearly with h_s. This is confirmed by our experimental results (Figure 3d). Having established a connection between our LSI results and a simple model for the drying kinetics, we now proceed with the same strategy to investigate the influence of environmental parameters that affect the drying kinetics.

2.4. Open Time versus Relative Humidity

Humidity has a profound effect on the drying dynamics of aqueous systems, and hence, it strongly influences the open time of waterborne paints. To capture this effect in a quantitative manner using our LSI-based approach, the relative humidity needs to be incorporated as a parameter in the equations for the evaporation kinetics. To that end, we write the vapor pressure as $p_v = H_R p_s$, with p_s the saturated vapor

https://doi.org/10.1021/acsaom.4c00051
ACS Appl. Opt. Mater. 2024, 2, 750−760

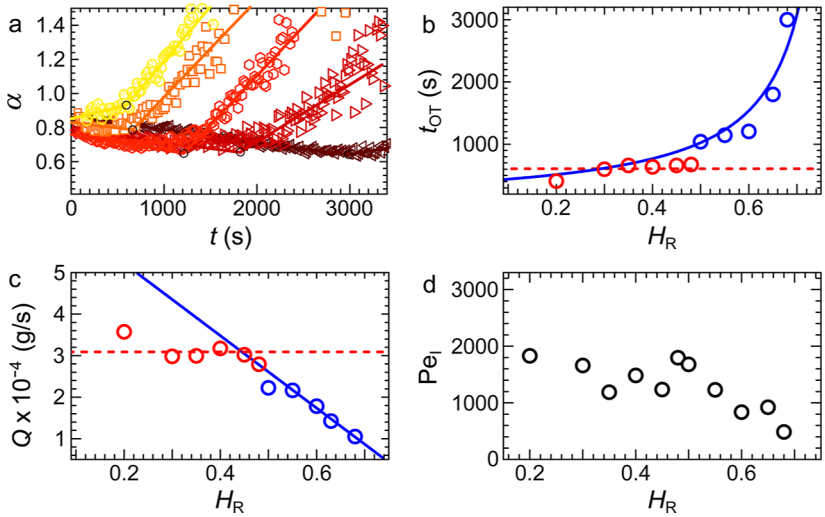

Figure 4. Open time as a function of relative humidity. (a) Temporal evolution of α for 200 μm paint films at H_R = 0.3 (yellow ○), 0.45 (orange □), 0.50 (red ⬡), 0.60 (red ▷), and 0.68 (brown ◁). (b) Open time versus relative humidity. The experimental data obtained for $H_R \geq 0.5$ (blue ○) are in good agreement with the prediction according to eq 8 (blue —). Due to skin formation, the open time exhibits a sharp drop and barely changes for $H_R < 0.5$ (red ○). (c) Evaporation rate versus relative humidity. The experimental results are in accordance with the expected scaling $Q \propto (a - H_R)$ (blue —) for $H_R \geq 0.5$ (blue ○) but attain a constant value at $H_R < 0.45$ (red ○), suggestive of skin formation. (d) Peclet number for freshly deposited paint films versus relative humidity.

pressure and H_R the relative humidity. This leads to $Q \propto (a - H_R)p_s$, where we have introduced an activity parameter $a = p_{eq}/p_s$, which corrects for deviations of the water activity from ideal values due to the composition of the paint film. For films with equal initial thickness and composition and with the same mass fraction ϕ_{OT} at the end of the open time, we thus expect the open time to scale as

$$t_{OT} \propto \frac{1}{(a - H_R)p_s} \tag{8}$$

To test this prediction, we examine the temporal evolution of α for different values of H_R (Figure 4a). We determine $t_{OT}(H_R)$ from the characteristic kink in the $\alpha(t)$ curves and fit these experimental values to eq 8, with a as an adjustable parameter (here we find a = 0.8). Interestingly, the theoretical prediction holds for the upper range of relative humidities $H_R \geq 0.5$ but fails to accurately describe the experimental data in the lower range $H_R < 0.5$ (Figure 4b). Notably, the open time drops abruptly at $H_R \approx 0.48$ and barely changes below this humidity. This discontinuity in $t_{OT}(H_R)$ hints at the advent of an additional phenomenon that alters the drying dynamics. Indeed, lower relative humidities enhance the drying kinetics which in turn could (i) facilitate particle packing at a ϕ_{OT} value different from the value observed for more humid air[42−45] or (ii) induce the formation of a thin solid-like layer called "skin" at the dispersion−air interface.[10,46−48] Such a skin consists of accumulated, coalesced polymer particles and thus forms a barrier for water evaporation. The occurrence of both phenomena could account for the sudden drop and the subsequent constant value of the open time at low H_R. To pinpoint the culprit for our experimental observations, we first identify a characteristic signature for each of the proposed phenomena. If a skin layer is formed at $H_R < 0.5$, the water transport through the dispersion−air interface should be significantly impeded by the presence of a semisolid layer there. Thus, we would expect the change in the evaporation rate Q to exhibit different regimes at low and high humidities. By contrast, a different packing at ϕ_{OT} should not interfere with the water evaporation as the size of the voids between the colloidal particles in a close-packing configuration is still much bigger than the size of water molecules. Thus, the water transport toward the dispersion−air interface should not be hindered and the change in Q should follow the same trend throughout the full range of experimental conditions used. As discussed above, we expect the evaporation rate to depend linearly on the relative humidity: $Q \propto (a - H_R)$. We indeed observe this experimentally for $H_R \geq 0.5$ (Figure 4c). However, for $H_R < 0.45$, the change in the experimentally determined evaporation rate deviates significantly from the linear regime observed at high humidities. In fact, the value of Q barely changes and remains close to constant at low H_R (Figure 4c). Such behavior is in line with the scenario of skin formation. To further assess the likelihood of this scenario, we estimate the initial Peclet number Pe_I for the paint film at the beginning of the drying process (see the Supporting Information). The Pe_I values are larger than unity for the whole H_R range, implying that the system is predisposed to skin formation (Figure 4d). Nevertheless, our measurements indicate that a skin is formed exclusively at $H_R \lesssim 0.5$. Most likely, only in this regime is the disjoining pressure—the force that counters breaching of the liquid film separating the particles—overcome by the pressure of the evaporation-induced packing, leading to coalescence (see Figure S1 and the corresponding discussion in the Supporting Information).[49] Both findings—the nonuniform dependence of the evaporation rate on relative humidity and the high Peclet numbers—strongly suggest that skin formation is at the root of the discrepancy between the measured t_{OT} and the prediction of eq 8.

3. OPEN TIME VERSUS TEMPERATURE

Temperature is another crucial environmental parameter that has strong effects on the drying of aqueous systems. To quantify these effects, we need to consider how the temperature affects the evaporation rate. In eq 5, which holds in the diffusion-limited regime, the diffusion coefficient

https://doi.org/10.1021/acsaom.4c00051
ACS Appl. Opt. Mater. 2024, 2, 750−760

depends on temperature (typically, $D \sim T^{3/2}$ for diffusion in the gas phase, which would lead to a scaling $Q \sim \sqrt{T}$. In the transfer-limited regime (eq 6), by contrast, we find $Q \sim 1/\sqrt{T}$. However, we should also account for the temperature dependence of the equilibrium vapor pressure p_s. This temperature dependence is given by the Clausius−Clapeyron equation: $d \ln p_s/dT = \Delta H_v/RT^2$, with ΔH the latent heat of evaporation and R the gas constant. For evaporation of water, we need to take into account that the latent heat depends on temperature, which makes integration of the Clausius−Clapeyron equation difficult. However, an accurate empirical approximation at standard atmospheric conditions is given by the August−Roche−Magnus equation[50]

$$p_s = 610\exp\left(\frac{17.3T_c}{T_c + 243.3}\right) \tag{9}$$

where T_c is the temperature in °C and the pressure is expressed in Pa. The temperature dependence of p_s as described by this equation overshadows the $\sqrt{T}$ dependence in eqs 5 and 6, so that we expect the following relation between the open time and the temperature

$$t_{OT} \approx c\exp\left(-\frac{17.3T_c}{T_c + 243.3}\right) \tag{10}$$

with c a prefactor (whose weak temperature dependence we ignore). Remarkably, only adjusting this parameter yields a prediction that perfectly falls in line with our experimental data for t_{OT} at different temperatures (Figure 5). The good agreement between the predictions and our experimental results indicates that the most relevant effects are apparently captured by our LSI-based approach.

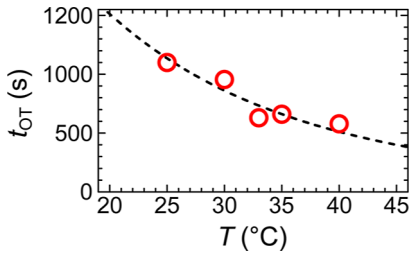

Figure 5. Open time as a function of temperature. The symbols represent the experimental data while the dashed line shows the theoretical prediction according to eq 10.

4. BEYOND THE OPEN TIME

We have shown that LSI allows us to closely follow the dynamics in the early stages of drying colloidal coatings and to determine an important quantity such as the open time. However, other phenomena that populate the later drying stages are of equal importance for the terminal state of the paint film. The question now arises if LSI can also be used to monitor these later events. At the heart of a film formation in water-based coatings is the process of phase inversion, in which the binder particles coalesce and give rise to a continuous polymer phase with any residual water dispersed in it as droplets. After the binder particles have attained close packing and undergone deformation, coalescence commences with the breakage of the thin water films that disjoin the highly deformed particles. This rupture is caused by the capillary forces that continuously grow with the ongoing solvent evaporation and at a certain point, exceed the disjoining pressure that keeps the soft colloids apart. Once the thin film fails, the contents of the particles are free to intermix. In situ methods to study the process of phase inversion in a spatially resolved manner are scarce. It is challenging to detect coalescence events by simply looking for structural changes since there is no clear macroscopic difference between strongly deformed and coalesced particles. In some cases, microscopy approaches have been deployed to monitor particle deformation and coalescence,[51−54] but their application becomes limited if the studied system is opaque and once the size of the coalescing particles approaches the diffraction limit, which is almost always true for realistic coating formulations. In other cases, small-angle scattering approaches (SAXS and SANS) have been used to follow film formation,[55,56] albeit in a spatially averaged manner.

To circumvent these challenges, we use LSI as an approach that relies on dynamics rather than structure to generate contrast and visualize the film formation process in opaque latex coatings. We start by mapping the dynamics in drying acrylic−styrene emulsion paints with different concentrations of coalescing aids (see the Experimental section). The d_2 maps for an emulsion paint containing 2.7 wt % coalescent reveal a sudden enhancement in the dynamics long beyond the open time (Figure 6a,b). This enhancement manifests itself as a well-defined front (Figure 6c) and is followed by a rapid decrease in the mobility (Figure 6d). To dissect this sequence of events in a more quantitative manner, we compute the temporal evolution of the field correlation function over extended periods. As time progresses, $g_1(\tau)$ shifts to 2 orders-of-magnitude longer τ-values, indicating a significant retardation of the dynamics (Figure 6e). We subsequently extract the relaxation time τ_0 and process identifier α by fitting $g_1(\tau)$ to eq 4.

Close examination of the τ_0 curves allows us to identify four distinct drying stages for all coalescent concentrations (Figure 6f). Stage I is essentially the open time period of the paint. Stage II is marked by a transient decrease of τ_0, implying enhanced motion. Most likely, the rising capillary pressure compresses and deforms the soft binder particles. This deformation translates into a macroscopic contraction of the paint imposing a net translational motion to the scattering TiO_2 particles downward and toward the center of the drying paint film. Once the capillary pressure exceeds the disjoining pressure, the drying process advances to stage III, in which the interstitial water films rupture and phase inversion takes place. After particle coalescence, the TiO_2 particles inhabit a continuous polymer phase with a significantly higher effective viscosity, which is reflected by the steep rise in τ_0. Additionally, the motion of the particles shifts to a more diffusive mode. The onset of the rapid rise in the τ_0 curve marks the time point to which we refer as the film formation time t_{FFT}. In the final stage IV, the coalescing aids slowly evaporate from the film, causing the viscosity to gradually increase and the mobility of the TiO_2 particles to drop further. The resultant rise in τ_0 continues over many hours to days (Figure 6f, inset). The temporal behavior of τ_0 and the d_2 maps are well in agreement with each other. The rapid increase in τ_0 implies that coalescence must occur across a sharp front, as was found previously.[57−59] We indeed observe this clearly in the d_2 maps for the emulsion paint 2.7 wt % coalescent at $t = t_{FFT}$. A well-defined gradient in mobility (Figure 6c) traverses through the field of view (Supporting

https://doi.org/10.1021/acsaom.4c00051
ACS Appl. Opt. Mater. 2024, 2, 750−760

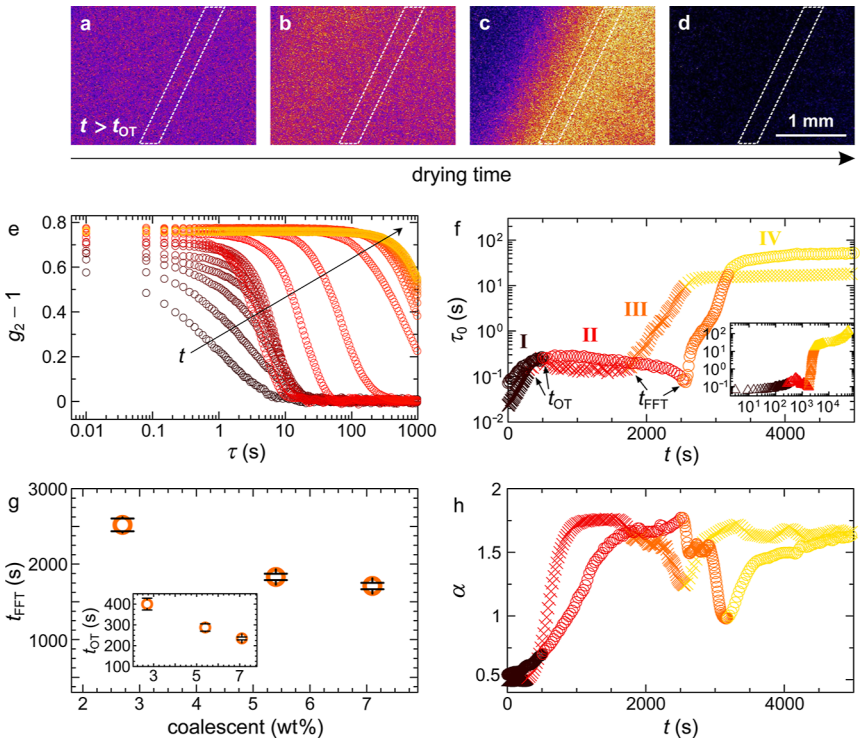

Figure 6. Quantification of film formation time and its dependence on coalescent concentration. (a–d) $d_2(\tau = 2\ s)$ maps of a 100 μm emulsion paint films with 2.7 wt % coalescent at different time points beyond the open time, capturing the film formation dynamics: t = 2545 s (a), 2550 s (b), 2555 s (c), and 2563 s (d). At $t = t_{FFT}$ = 2555 s, a clear coalescence front passes (c). The dashed lines delineate the region of interest. The scale bar applies to all images. (e) Typical correlation functions over time for the paint formulations containing 2.7 wt % coalescent, showing a distinct crossover and change of shape upon film formation. The time interval between consecutive curves is 5 min. (f) Temporal evolution of the characteristic relaxation time for 2.7 wt % (○) and 7.1 wt % (×) coalescent. The Roman numbers and colors designate the four drying stages described in the main text. The inset in (f) shows a long-term measurement of τ_0 for emulsion paint with 5.4 wt % coalescent. (g) Film formation time and open time (inset) as a function of coalescent concentration. Each data point is the average of two measurements; the error bars represent the standard deviations. (h) Temporal evolution of the process identifier.

Information Video). This front is truly a dynamic transition and cannot be identified on the basis of structural features, e.g., relying on absolute intensity (Figure S3a). Our interpretations are further supported by the $\alpha(t)$ curves. The significant increase of α in stage II implies a shift to (super)ballistic dynamics (Figure 6h), which is in line with the stipulated collective translation of the particles caused by the contracting paint. High stretching exponents are relatively unusual but have previously been attributed to relaxation of internal stresses in jammed colloidal systems.[60,61] Interestingly, in stage III, we observe a rapid drop in α after the film formation time (Figure 6h). This sharp decrease in α combined with the kink in τ_0 is consistent with our hypothesis that across the coalescence front, the TiO_2 particles shift from accelerating translation to more diffusive dynamics, which may well be the signature of coalescence in a coating.

Even though the overall shapes of the τ_0 and α curves are the same for different coalescent concentrations, they are clearly shifted along the time axis (Figure 6f,h). Surprisingly, adding coalescing aids considerably decreases the open time (Figure 6g, inset); this is an undesired effect, which is important to take into account when formulating paints. We attribute this effect to the partitioning of coalescing aids into the polymer particles. As a consequence, the binder particles swell, and close packing is reached at an earlier time point. Dynamic light scattering measurements confirm this difference in particle sizes: the samples with 2.7 and 7.1 wt % coalescent exhibit particle diameters of 124 and 142 nm, respectively.

Not only the open time decreases upon increasing the coalescent concentration, but the film formation time also decreases even more (Figure 6g), which is the intended result. Coalescing aids are commonly added to plasticize the binder particles by increasing the free volume of the polymer chains.[62−64] The earlier onset of coalescence is further enhanced by the swelling-induced increase in the volume fraction of the latex particles. Another consequence is the absence of a sharp coalescence front in the strongly plasticized paint film (7.1 wt % coalescent), which instead is much more gradual and delocalized (compare Figure S3b,c). These observations are in agreement with previous work on drying surfactant-stabilized oil-in-water emulsions, which revealed two distinct modes of coalescence: “front coalescence” at high surfactant concentrations (stable emulsions) versus “bulk coalescence” at low surfactant concentrations (unstable emulsions).[65] In the first scenario, a steep gradient in the capillary pressure is required to induce coalescence, which thus takes place at only at the drying end of the emulsion where the high capillary pressure condition is met. In the second scenario, a lower capillary pressure is already sufficient to induce coalescence, which thus occurs simultaneously at many locations in the bulk. These results are analogous to the findings in our work, where instead we have varied the particle resistance to coalescence by changing the coalescent concentration.

Since the characteristic shape of $\tau_0(t)$ and the dip in $\alpha(t)$ are reproducible in all measurements and also for other latex

https://doi.org/10.1021/acsaom.4c00051
ACS Appl. Opt. Mater. 2024, 2, 750−760

systems, these features may serve as a standard approach to extract the film formation time in drying waterborne coatings. The small standard deviations in t_{FFT} derived from the onset of the abrupt decrease in α highlight the robustness of this procedure (Figure 6g). Although the observed strong dependence of coalescence on the coalescent concentration is in line with expectations and earlier research,[62−64] we now have a straightforward and easily adaptable method to quantify the film formation time unambiguously. An inherent limitation of LSI is its lack of depth-resolved data. Coatings are unlikely to be vertically homogeneous, hence film formation will be more complex in reality. The development of 3D LSI techniques holds promise for further investigation of these potential variations in future studies.

5. CONCLUSIONS

In this study, we have deployed LSI as a versatile tool for a quantitative characterization of drying waterborne coatings. As such, LSI enables us to objectively determine the open time of realistic paint formulations for a wide range of drying conditions. The excellent agreement between our experimental observations for the open time and the scaling predictions derived from well-established evaporation rate theory not only validates our LSI approach for open-time determination but also allows accurate predictions for the behavior of this quantity in the whole set of conditions used in this work. Furthermore, the advent of deviations from the expected behavior permits the detection of undesired phenomena that might occur during drying, such as skin formation. A direct comparison of the LSI-based open time and the open time determined using other established techniques in the future will facilitate further validation and the establishment of LSI as reliable and objective approach for open time determination of water-based paints. In this work, we have also shown how the wide temporal dynamic range of LSI makes it possible to extend our quantitative observations toward longer time scales populated by other relevant processes, namely, the deformation of binder particles in later stages and their subsequent coalescence into a solid paint film. LSI allows us not only to determine the time point at which the water-dispersed polymer phase transitions to a continuous polymer phase but also to monitor the propagation of the coalescence front in a spatiotemporally resolved manner. These results highlight the potential role of this method in the detailed study of drying stages in water-based coatings and could aid in the rational design of waterborne paints with a tailored drying profile.

6. EXPERIMENTAL SECTION

6.1. Experimental Setup

All measurements are performed on a custom-built instrument, which is represented schematically in Figure 1a. The sample holder resides within an insulated chamber where temperature and relative humidity are precisely controlled at desired values. A continuous flow of dry and water-saturated air, mixed in adjustable ratios at the chamber inlet, maintains these conditions. Three external thermistor probes (TSP01, Thorlabs) continuously monitor T and RH, with the data logged via USB using custom software that provides feedback for controlling the air mixture. To minimize directional convective fluxes within the chamber, the inlet air is diffused through a large number of small holes in the tubing. This also facilitates the continuous refreshment of the chamber atmosphere, preventing stagnation. Unless specified otherwise, T = 25 °C and H_R = 0.5. The holder is coupled to a computer-controlled analytical balance (WZA224-NC, Sartorius) which allows for continuous monitoring of the sample mass. A 532 nm solid-state laser (Samba 1W, Cobolt) is used as the light source. The laser beam is first driven through a half-wave plate and then through a polarizing beam splitter in order to adjust the intensity. Subsequently, the light is guided through a beam expander to set the cross-sectional size of the beam to $d \sim 1$ cm. The resulting beam is navigated via mirrors toward the sample. The backscattered light from the sample first passes through a polarizer which filters the reflected photons and photons with short paths. Finally, the filtered backscattered light is collected by a zoom lens (1.8 ×) and focused on a CCD camera (Dalsa Genie, CR-GM00-H640x, Stemmer Imaging). The speckle size is set 2−3 times bigger than the physical size of the camera pixels to ensure a good balance between spatial resolution and signal-to-noise ratio.[26] All speckle images are acquired at 100 fps with the exposure time optimized to exploit the full dynamic range of the camera. To minimize edge effects on our open time measurements, we have performed all our LSI measurements in the center of the film.

6.2. Data Analysis

To study the ongoing dynamics in the drying coatings, we compute the intensity structure function d_2, the intensity correlation function g_2, and the field correlation function g_1 using eqs 1, 2, and 3, respectively. The spatial correlation factor β, which accounts for the number of speckles per camera pixel ($0 < \beta \leq 1$), is chosen such that $g_2 - 1 \rightarrow \beta$ for $\tau \rightarrow 0$. A value of 1.5 is used for the numerical prefactor γ, which has been experimentally determined elsewhere.[26]

6.3. Materials

All measurements are performed on commercial water-based paints (acrylic−styrene copolymer emulsions) supplied by DSM N.V. The effects of relative humidity and temperature are studied for 200 μm thick wet paint films deposited using a quadruple film applicator (Erichsen) that ensures well-defined dimensions (see the Supporting Information). The paint formulation includes 2.7 wt % butyldiglycol and texanol (2,2,4-trimethyl-1,3-pentanediol monoisobutyrate) as coalescing aids and 0.15 wt % TiO_2 (titania, DLS-derived d = 316 ± 8 nm and PDI = 0.2) as a strongly scattering pigment. These TiO_2 particles are isotropic, low-polydispersity, well-dispersed, and surface-treated with aluminum and zirconium compounds to promote durability. The initial water content is ∼60 wt %. Film formation in the later drying stages is studied for 100 μm thick wet paint films with varying total coalescent concentrations: 2.7 wt % (1.7 wt % butyldiglycol +1 wt % texanol), 5.4 wt % (3.4 wt % butyldiglycol +2 wt % texanol) and 7.2 wt % (5.1 wt % butyldiglycol +2 wt % texanol). The temperature and relative humidity are fixed at 23 ± 1 °C and 0.43 ± 0.02, respectively.

■ ASSOCIATED CONTENT

Supporting Information

The Supporting Information is available free of charge at https://pubs.acs.org/doi/10.1021/acsaom.4c00051.

Additional figures and discussions about the Peclet number estimation, the paint deposition method, and coalescence in the coatings (PDF)

d_2 video capturing coalescence in a coating (AVI)

■ AUTHOR INFORMATION

Corresponding Author

Joris Sprakel − *Physical Chemistry and Soft Matter, Wageningen University & Research, 6708 WE Wageningen, The Netherlands;* orcid.org/0000-0001-6532-4514; Email: joris.sprakel@wur.nl

Authors

Slav A. Semerdzhiev − *Physical Chemistry and Soft Matter, Wageningen University & Research, 6708 WE Wageningen, The Netherlands; Dutch Polymer Institute (DPI), 5600 AX*

https://doi.org/10.1021/acsaom.4c00051
ACS Appl. Opt. Mater. 2024, 2, 750−760

Eindhoven, The Netherlands; orcid.org/0000-0002-7594-0641

Hanne M. van der Kooij − *Physical Chemistry and Soft Matter, Wageningen University & Research, 6708 WE Wageningen, The Netherlands; Dutch Polymer Institute (DPI), 5600 AX Eindhoven, The Netherlands;* orcid.org/0000-0003-0441-1109

Remco Fokkink − *Physical Chemistry and Soft Matter, Wageningen University & Research, 6708 WE Wageningen, The Netherlands*

Jasper van der Gucht − *Physical Chemistry and Soft Matter, Wageningen University & Research, 6708 WE Wageningen, The Netherlands;* orcid.org/0000-0001-5525-8322

Complete contact information is available at: https://pubs.acs.org/10.1021/acsaom.4c00051

Notes

The authors declare no competing financial interest.

■ ACKNOWLEDGMENTS

This research forms part of the research programme of the Dutch Polymer Institute (DPI), projects 913ft16 and 781. We thank DSM for providing us with the different water-based paint formulations used in this work.

■ REFERENCES

(1) Embuscado, M. E.; Huber, K. C. *Edible Films and Coatings for Food Applications*; Springer, 2009.
(2) Hoath, S. D. *Fundamentals of Inkjet Printing: The Science of Inkjet and Droplets*; John Wiley & Sons, 2016.
(3) Keddie, J. L.; Routh, A. F. *Fundamentals of Latex Film Formation: Processes and Properties*; Springer, 2010.
(4) Wicks, Z. W.; Jones, F. N.; Peppas, S. P. *Organic Coatings: Science and Technology*; John Wiley & Sons: Chichester, 1992; p 259.
(5) Morrow, L. A.; Steinhauer, S. R. Alterations in heart rate and pupillary response in persons with organic solvent exposure. *Biol. Psychiatr.* **1995**, *37*, 721−730.
(6) Triebig, G.; Hallermann, J. Survey of solvent related chronic encephalopathy as an occupational disease in European countries. *Occup. Environ. Med.* **2001**, *58*, 575−581.
(7) Böckelmann, I.; Lindner, H.; Peters, B.; Pfister, E. A. Einfluss langjähriger beruflicher Lösemittelexposition auf das Farbensehen. *Der Ophthalmologe* **2003**, *100*, 133−141.
(8) Overbeek, A.; Bückmann, F.; Martin, E.; Steenwinkel, P.; Annable, T. New generation decorative paint technology. *Prog. Org. Coat.* **2003**, *48*, 125−139.
(9) Salamanca, J. M.; Ciampi, E.; Faux, D. A.; Glover, P. M.; McDonald, P. J.; Routh, A. F.; Peters, A. C. I. A.; Satguru, R.; Keddie, J. L. Lateral drying in thick films of waterborne colloidal particles. *Langmuir* **2001**, *17*, 3202−3207.
(10) Carter, F. T.; Kowalczyk, R. M.; Millichamp, I.; Chainey, M.; Keddie, J. L. Correlating particle deformation with water concentration profiles during latex film formation: Reasons that softer latex films take longer to dry. *Langmuir* **2014**, *30*, 9672−9681.
(11) Zhou, C.; Yu, G.; Furuya, D.; Greenberg, J. H.; Yodh, A. G.; Durduran, T. Diffuse optical correlation tomography of cerebral blood flow during cortical spreading depression in rat brain. *Opt. Express* **2006**, *14*, 1125−1144.
(12) Zakharov, P.; Völker, A.; Wyss, M. T.; Haiss, F.; Calcinaghi, N.; Zunzunegui, C.; Buck, A.; Scheffold, F.; Weber, B. Dynamic laser speckle imaging of cerebral blood flow. *Opt. Express* **2009**, *17*, 13904−13917.
(13) Draijer, M.; Hondebrink, E.; van Leeuwen, T.; Steenbergen, W. Review of laser speckle contrast techniques for visualizing tissue perfusion. *Lasers Med. Sci.* **2009**, *24*, 639−651.
(14) Pajuelo, M.; Baldwin, G.; Rabal, H.; Cap, N.; Arizaga, R.; Trivi, M. Bio-speckle assessment of bruising in fruits. *Opt. Lasers Eng.* **2003**, *40*, 13−24.
(15) Maksymenko, O. P.; Muravsky, L. I.; Berezyuk, M. I. Application of biospeckles for assessment of structural and cellular changes in muscle tissue. *J. Biomed. Opt.* **2015**, *20*, 095006.
(16) Hajjarian, Z.; Nadkarni, S. K. Evaluating the viscoelastic properties of tissue from laser speckle fluctuations. *Sci. Rep.* **2012**, *2*, 316.
(17) Erpelding, M.; Amon, A.; Crassous, J. Diffusive wave spectroscopy applied to the spatially resolved deformation of a solid. *Phys. Rev. E* **2008**, *78*, 046104.
(18) Hinsch, K. D.; Fricke-Begemann, T.; Gülker, G.; Wolff, K. Speckle correlation for the analysis of random processes at rough surfaces. *Opt. Lasers Eng.* **2000**, *33*, 87−105.
(19) Koshoji, N. H.; Bussadori, S. K.; Bortoletto, C. C.; Prates, R. A.; Oliveira, M. T.; Deana, A. M. Laser speckle imaging: a novel method for detecting dental erosion. *PLoS One* **2015**, *10*, No. e0118429.
(20) van der Kooij, H. M.; Semerdzhiev, S. A.; Buijs, J.; Broer, D. J.; Liu, D.; Sprakel, J. Morphing of liquid crystal surfaces by emergent collectivity. *Nat. Commun.* **2019**, *10*, 3501.
(21) van der Kooij, H. M.; Broer, D. J.; Liu, D.; Sprakel, J. Electroplasticization of liquid crystal polymer networks. *ACS Appl. Mater. Interfaces* **2020**, *12*, 19927−19937.
(22) Wu, Q.; Buijs, J.; de Groot, S.; van der Kooij, H. M.; van der Gucht, J.; Kodger, T. E. Spatially heterogenous dynamics in colloidal gels during syneresis. *Soft Matter* **2023**, *19*, 5336−5344.
(23) Buijs, J. J.; Fix, R.; van der Kooij, H. M.; Kodger, T. E. Real-time imaging of bonding in 3D-printed layers. *JoVE* **2023**, No. e65415.
(24) Colijn, I.; Postma, E.; Fix, R.; van der Kooij, H. M.; Schroën, K. Particle dispersion governs nano to bulk dynamics for tailored nanocomposite design. *J. Colloid Interface Sci.* **2024**, *658*, 354−361.
(25) Pine, D. J.; Weitz, D. A.; Zhu, J. X.; Herbolzheimer, E. Diffusing-wave spectroscopy: dynamic light scattering in the multiple scattering limit. *J. Phys.* **1990**, *51*, 2101−2127.
(26) van der Kooij, H. M.; Fokkink, R.; van der Gucht, J.; Sprakel, J. Quantitative imaging of heterogeneous dynamics in drying and aging paints. *Sci. Rep.* **2016**, *6*, 34383.
(27) Schulz-DuBois, E. O.; Rehberg, I. Structure function in lieu of correlation function. *Appl. Phys.* **1981**, *24*, 323−329.
(28) Schätzel, K. Correlation techniques in dynamic light scattering. *Appl. Phys. B: Laser Opt.* **1987**, *42*, 193−213.
(29) Lorusso, G. F.; Minafra, A.; Capozzi, V. Noise dependence of correlation and structure functions on mean count rate and sampling time. *Appl. Opt.* **1993**, *32*, 3867−3870.
(30) Guo, H.; Bourret, G.; Lennox, R. B.; Sutton, M.; Harden, J. L.; Leheny, R. L. Entanglement-controlled subdiffusion of nanoparticles within concentrated polymer solutions. *Phys. Rev. Lett.* **2012**, *109*, 055901.
(31) Weitz, D. A.; Pine, D. J.; Pusey, P. N.; Tough, R. J. A. Nondiffusive Brownian motion studied by diffusing-wave spectroscopy. *Phys. Rev. Lett.* **1989**, *63*, 1747−1750.
(32) Brun, A.; Brunel, L.; Snabre, P. Adaptive speckle imaging interferometry (ASII): New technology for advanced drying analysis of coatings. *Surf. Coat. Int., Part B* **2006**, *89*, 251−254.
(33) Brun, A.; Dihang, H.; Brunel, L. Film formation of coatings studied by diffusing-wave spectroscopy. *Prog. Org. Coat.* **2008**, *61*, 181−191.
(34) Giraud, I.; Dantras, E.; Brun, A.; Dihang, H.; Brunel, L.; Bernès, A.; Meunier, G.; Lacabanne, C. Film formation analysis by diffusive wave spectroscopy. *Prog. Org. Coat.* **2009**, *64*, 515−519.
(35) Keddie, J. L. Film formation of latex. *Mater. Sci. Eng. R Rep.* **1997**, *21*, 101−170.
(36) van der Kooij, H. M.; van de Kerkhof, G. T.; Sprakel, J. A mechanistic view of drying suspension droplets. *Soft Matter* **2016**, *12*, 2858−2867.

(37) Mason, T. G.; Ganesan, K.; van Zanten, J. H.; Wirtz, D.; Kuo, S. C. Particle Tracking Microrheology of Complex Fluids. *Phys. Rev. Lett.* **1997**, *79*, 3282−3285.
(38) Jones, F. E. *Evaporation of Water With Emphasis on Applications and Measurements*; CRC Press, 1992.
(39) Langmuir, I. Vapor pressures, evaporation, condensation, and adsorption. *J. Am. Chem. Soc.* **1932**, *54*, 2798−2832.
(40) Knudsen, M. *The Kinetic Theory of Gases: Some Modern Aspects*; Methuen & Company, 1950.
(41) Hertz, H. Ueber die Verdunstung der Flüssigkeiten, insbesondere des Quecksilbers, im luftleeren Raume. *Ann. Phys.* **1882**, *253* (10), 177−193.
(42) Routh, A. F.; Zimmerman, W. B. Distribution of particles during solvent evaporation from films. *Chem. Eng. Sci.* **2004**, *59*, 2961−2968.
(43) Marín, Á. G.; Gelderblom, H.; Lohse, D.; Snoeijer, J. H. Order-to-disorder transition in ring-shaped colloidal stains. *Phys. Rev. Lett.* **2011**, *107*, 085502.
(44) Piroird, K.; Lazarus, V.; Gauthier, G.; Lesaine, A.; Bonamy, D.; Rountree, C. L. Role of evaporation rate on the particle organization and crack patterns obtained by drying a colloidal layer. *Europhys. Lett.* **2016**, *113*, 38002.
(45) Noirjean, C.; Marcellini, M.; Deville, S.; Kodger, T. E.; Monteux, C. Dynamics and ordering of weakly Brownian particles in directional drying. *Phys. Rev. Mater.* **2017**, *1*, 065601.
(46) Sheetz, D. P. Formation of films by drying of latex. *J. Appl. Polym. Sci.* **1965**, *9*, 3759−3773.
(47) König, A. M.; Weerakkody, T. G.; Keddie, J. L.; Johannsmann, D. Heterogeneous drying of colloidal polymer films: dependence on added salt. *Langmuir* **2008**, *24*, 7580−7589.
(48) Wahdat, H.; Hirth, C.; Johannsmann, D.; Gerst, M.; Rückel, M.; Adams, J. Film Formation of Pressure-Sensitive Adhesives (PSAs) Studied with Förster Resonance Energy Transfer (FRET) and Scattering Intensity. *Macromolecules* **2018**, *51*, 4718−4726.
(49) Feng, H.; Sprakel, J.; van der Gucht, J. Hydrodynamic model for drying emulsions. *Phys. Rev. E* **2015**, *92*, 023011.
(50) Alduchov, O. A.; Eskridge, R. E. Improved Magnus form approximation of saturation vapor pressure. *J. Appl. Meteorol.* **1996**, *35*, 601−609.
(51) Mchugh, A. J.; Tsay, C. S. Dynamics of the phase inversion process. *J. Appl. Polym. Sci.* **1992**, *46*, 2011−2021.
(52) Charin, R. M.; Nele, M.; Tavares, F. W. Transitional Phase Inversion of Emulsions Monitored by in Situ Near-Infrared Spectroscopy. *Langmuir* **2013**, *29*, 5995−6003.
(53) Gonzalez, E.; Tollan, C.; Chuvilin, A.; Barandiaran, M. J.; Paulis, M. Determination of the Coalescence Temperature of Latexes by Environmental Scanning Electron Microscopy. *ACS Appl. Mater. Interfaces* **2012**, *4*, 4276−4282.
(54) Krebs, T.; Ershov, D.; Schroen, C. G. P. H.; Boom, R. M. Coalescence and compression in centrifuged emulsions studied with in situ optical microscopy. *Soft Matter* **2013**, *9*, 4026−4035.
(55) Chevalier, Y.; Pichot, C.; Graillat, C.; Joanicot, M.; Wong, K.; Maquet, J.; Lindner, P.; Cabane, B. Film formation with latex particles. *Colloid Polym. Sci.* **1992**, *270*, 806−821.
(56) Vagias, A.; Chen, Q.; ten Brink, G. H.; Hermida-Merino, D.; Scheerder, J.; Portale, G. Investigation of the nanoscale morphology in industrially relevant clearcoats of waterborne polymer colloids by means of variable-angle grazing incidence small-angle X-ray scattering. *ACS Appl. Mater. Interfaces* **2019**, *1*, 2482−2494.
(57) Ma, Y.; Davis, H. T.; Scriven, L. E. Microstructure development in drying latex coatings. *Prog. Org. Coat.* **2005**, *52*, 46−62.
(58) Haley, J. C.; Liu, Y.; Winnik, M. A.; Lau, W. The onset of polymer diffusion in a drying acrylate latex: how water initially retards coalescence but ultimately enhances diffusion. *J. Coat. Technol. Res.* **2008**, *5*, 157−168.
(59) van der Kooij, H. M.; de Kool, M.; van der Gucht, J.; Sprakel, J. Coalescence, Cracking, and Crack Healing in Drying Dispersion Droplets. *Langmuir* **2015**, *31*, 4419−4428.
(60) Cipelletti, L.; Ramos, L.; Manley, S.; Pitard, E.; Weitz, D. A.; Pashkovski, E. E.; Johansson, M. Universal non-diffusive slow dynamics in aging soft matter. *Faraday Discuss.* **2003**, *123*, 237−251.
(61) Cipelletti, L.; Ramos, L. Slow dynamics in glassy soft matter. *J. Phys.: Condens. Matter* **2005**, *17*, R253−R285.
(62) Schroeder, W. F.; Liu, Y.; Tomba, J. P.; Soleimani, M.; Lau, W.; Winnik, M. A. Influence of Ethylene Glycol and Propylene Glycol on Polymer Diffusion in Poly(butyl acrylate-co-methyl methacrylate) Latex Films. *J. Phys. Chem. B* **2010**, *114*, 3085−3094.
(63) Divry, V.; Gromer, A.; Nassar, M.; Lambour, C.; Collin, D.; Holl, Y. Drying Mechanisms in Plasticized Latex Films: Role of Horizontal Drying Fronts. *J. Phys. Chem. B* **2016**, *120*, 6791−6802.
(64) Berce, P.; Skale, S.; Razboršek, T.; Slemnik, M. Influence of coalescing aids on the latex properties and film formation of waterborne coatings. *J. Appl. Polym. Sci.* **2017**, *134*, 45142.
(65) Feng, H.; Sprakel, J.; Ershov, D.; Krebs, T.; Cohen Stuart, M. A.; van der Gucht, J. Two modes of phase inversion in a drying emulsion. *Soft Matter* **2013**, *9*, 2810−2815.

https://doi.org/10.1021/acsaom.4c00051
ACS Appl. Opt. Mater. 2024, 2, 750−760